

1 Author responses in red.

2
3 Dear authors,

4 Thank you for your very thorough response to the reviewers' comments. I have a few very
5 minor points that I would like to see addressed before I can recommend your manuscript for
6 publication.

7 Thank you for your comments.

8
9 - The use of R2 is a bit imprecise. Typically, the coefficient of determination is used as an
10 indicator for the correlation between two datasets. However, in some places (e.g lines 590-
11 594, 719-723) the two datasets are not explicitly stated. Presumably, it is observations vs.
12 model results but it would be a help to the reader if this was clarified (e.g. similar to what is
13 stated in lines 643-646).

14 We have clarified the datasets that are the basis for these R² calculations.

15
16 - The figures showing maps of the two glacier (Figs. 3, 8,10 and 11) would be easier to read if
17 a "G" and "W" were added (if possible).

18 We have added text labels "Wolverine and Gulkana" to Figure 3 to improve readability of this
19 and subsequent figures.

20
21 - In response to reviewer #1 's comment to line 642, please state that details on interpolation
22 scheme and geodetic calibrations can be found in van Beusekom et al., 2010 and O'Neel et al.,
23 2014.

24 We have added these references in the requested location.

25
26 - I agree with M. Pelto's request to line 387 re. mentioning how much the observed
27 observations exceeded model results. In view of the large amount of data, it would be
28 sufficient to give an example so the reader has an idea of the magnitude of the values.
29 Something along the lines of "For example, in 2015 observed SWE exceeded modelled SWE by
30 more/less than X amount for Y% of data points".

31 We have added the suggested calculation for a year as an example of the residual variability.

32
33 I hope that you are willing to incorporate these changes so we can move forward with your
34 interesting study.

35 Best,
36 Nanna

37

38

39

40

41

42

43

44

45

46

47

48

49 **Interannual snow accumulation variability on glaciers derived from repeat,**
50 **spatially extensive ground-penetrating radar surveys**

51

52 Daniel McGrath¹, Louis Sass², Shad O'Neel² Chris McNeil², Salvatore G. Candela³,
53 Emily H. Baker², and Hans-Peter Marshall⁴

54 ¹*Department of Geosciences, Colorado State University, Fort Collins, CO*

55 ²*U.S. Geological Survey Alaska Science Center, Anchorage, AK*

56 ³*School of Earth Sciences and Byrd Polar Research Center, Ohio State University,*
57 *Columbus, OH*

58 ⁴*Department of Geosciences, Boise State University, Boise, ID*

59 **Abstract**

60 There is significant uncertainty regarding the spatiotemporal distribution of seasonal
61 snow on glaciers, despite being a fundamental component of glacier mass balance. To
62 address this knowledge gap, we collected repeat, spatially extensive high-frequency
63 ground-penetrating radar (GPR) observations on two glaciers in Alaska during the spring
64 of five consecutive years. GPR measurements showed steep snow water equivalent
65 (SWE) elevation gradients at both sites; continental Gulkana Glacier's SWE gradient
66 averaged 115 mm 100 m⁻¹ and maritime Wolverine Glacier's gradient averaged 440 mm
67 100 m⁻¹ (over >1000 m). We extrapolated GPR point observations across the glacier
68 surface using terrain parameters derived from digital elevation models as predictor
69 variables in two statistical models (stepwise multivariable linear regression and
70 regression trees). Elevation and proxies for wind redistribution had the greatest
71 explanatory power, and exhibited relatively time-constant coefficients over the study
72 period. Both statistical models yielded comparable estimates of glacier-wide average
73 SWE (1 % average difference at Gulkana, 4 % average difference at Wolverine),
74 although the spatial distributions produced by the models diverged in unsampled regions
75 of the glacier, particularly at Wolverine. In total, six different methods for estimating the
76 glacier-wide winter balance average agreed within ± 11 %. We assessed interannual
77 variability in the spatial pattern of snow accumulation predicted by the statistical models
78 using two quantitative metrics. Both glaciers exhibited a high degree of temporal
79 stability, with ~85 % of the glacier area experiencing less than 25 % normalized absolute
80 variability over this five-year interval. We found SWE at a sparse network (3 stakes per
81 glacier) of long-term glaciological stake sites to be highly correlated with the GPR-
82 derived glacier-wide average. We estimate that interannual variability in the spatial
83 pattern of winter SWE accumulation is only a small component (4–10 % of glacier-wide
84 average) of the total mass balance uncertainty and thus, our findings support the concept

85 that sparse stake networks effectively measure interannual variability in winter balance
86 on glaciers, rather than some temporally varying spatial pattern of snow accumulation.

87

88 1. Introduction

89 Our ability to quantify glacier mass balance is dependent on accurately resolving the
90 spatial and temporal distributions of snow accumulation and snow/ice ablation.

91 Significant advances in our knowledge of ablation processes have improved

92 observational and modelling capacities (Hock, 2005; Huss and Hock, 2015; Fitzpatrick et
93 al., 2017), yet comparable advances in our understanding of the distribution of snow

94 accumulation have not kept pace (Hock et al., 2017). Reasons for this discrepancy are

95 two-fold: (i) snow accumulation exhibits higher variability than ablation, both in

96 magnitude and length scale, largely due to wind redistribution in the complex high-relief

97 terrain where mountain glaciers are typically found (Kuhn et al., 1995) and (ii)

98 accumulation observations are typically less representative (i.e., one stake in a few

99 hundred meter elevation band) or less effective than comparable ablation observations

100 (i.e., precipitation gage measuring snowfall vs. radiometer measuring short-wave

101 radiation). This discrepancy presents a significant limitation to process-based

102 understanding of mass balance drivers. Furthermore, a warming climate has already

103 modified – and will continue to modify – the magnitude and spatial distribution of snow

104 on glaciers through a reduction in the fraction of precipitation falling as snow and an

105 increase in rain-on-snow events (McAfee et al., 2013; Klos et al., 2014; McGrath et al.,

106 2017; [Beamer et al., 2017](#); Littell et al., 2018).

107

108 Significant research has been conducted on the spatial and, to a lesser degree, the

109 temporal variability of seasonal snow in mountainous and high-latitude landscapes (e.g.,

110 Balk and Elder, 2000; Molotch et al., 2005; Erickson et al., 2005; Deems et al., 2008;

111 Sturm and Wagner, 2010; Schirmer et al., 2011; Winstral and Marks, 2014; Anderson et

112 al., 2014; Painter et al., 2016). Although major advances have occurred in applying

113 physically-based snow distribution models (i.e., iSnobal (Marks et al., 1999), SnowModel

114 (Liston and Elder, 2006), Alpine 3D (Lehning et al., 2006)), the paucity of required

115 meteorological forcing data proximal to glaciers limits widespread application. Many

116 other studies have successfully developed statistical approaches that rely on the

Deleted: Knowles et al., 2006;

118 relationship between the distribution of snow water equivalent (SWE) and physically-
119 based terrain parameters (also referred to as physiographic or topographic properties or
120 variables) to model the distribution of SWE across entire basins (e.g., Molotch et al.,
121 2005; Anderson et al., 2014; Sold et al., 2013; McGrath et al., 2015).

122
123 A major uncertainty identified by these studies is the degree to which these statistically
124 derived relationships remain stationary in time. Many studies (Erickson et al., 2005;
125 Deems et al., 2008; Sturm and Wagner, 2010; Schirmer et al., 2011; Winstral and Marks,
126 2014; Helfricht et al., 2014) have found ‘time-stability’ in the distribution of SWE,
127 including locations where wind redistribution is a major control on this distribution. For
128 instance, a climatological snow distribution pattern, produced from the mean of nine
129 standardized surveys, accurately predicted the observed snow depth in a subsequent
130 survey in a tundra basin in Alaska (~4–10 cm root mean square error (RMSE); Sturm and
131 Wagner, 2010). Repeat LiDAR surveys over two years at three hillslope-scale study plots
132 in the Swiss Alps found a high degree of correlation ($r=0.97$) in snow depth spatial
133 patterns (Schirmer et al., 2011). They found that the final snow depth distributions at the
134 end of the two winter seasons were more similar than the distributions of any two
135 individual storms during that two-year period (Schirmer et al., 2011). Lastly, an 11-year
136 study of extensive snow probing (~1200 point observations) at a 0.36 km² field site in
137 southwestern Idaho found consistent spatial patterns ($r=0.84$; Winstral and Marks, 2014).
138 Collectively, these studies suggest that in landscapes characterized by complex
139 topography and extensive wind redistribution of snow, spatial patterns are largely time-
140 stable or stationary, as long as the primary drivers are stationary.

141
142 Even fewer studies have explicitly examined the question of interannual variability in the
143 context of snow distribution on glaciers. Spatially-extensive snow probe datasets are
144 collected by numerous glacier monitoring programs (e.g., Bauder et al., 2017; Kjølmoen
145 et al., 2017; Escher-Vetter et al., 2009) in order to calculate a winter mass balance
146 estimate. Although extensive, such manual approaches are still limited by the number of
147 points that can be collected and uncertainties in correctly identifying the summer surface
148 in the accumulation zone, where seasonal snow is underlain by firn. One study of two

149 successive end-of-winter surveys of snow depth using probes on a glacier in Svalbard
150 found strong interannual variability in the spatial distribution of snow, and the
151 relationship between snow distribution and topographic features (Hodgkins et al., 2006).
152 Elevation was found to only explain 38–60 % of the variability in snow depth, and in one
153 year, snow depth was not dependent on elevation in the accumulation zone (Hodgkins et
154 al., 2006). Instead, aspect, reflecting relative exposure or shelter from prevailing winds,
155 was found to be a significant predictor of accumulation patterns. In contrast, repeat
156 airborne LiDAR surveys of a ~36 km² basin (~50% glacier cover) in Austria over five
157 winters found that the glacierized area exhibited less interannual variability (as measured
158 by the interannual standard deviation) than the non-glacierized sectors of the basin
159 (Helfricht et al., 2014). Similarly, a three-year study of snow distribution on
160 Findelgletscher in the Swiss Alps using ground-penetrating radar (GPR) found low
161 interannual variability, as 86 % of the glacier area experienced less than 25 % normalized
162 relative variability (Sold et al., 2016). These latter studies suggest that seasonal snow
163 distribution on glaciers likely exhibits ‘time-stability’ in its distribution, but few datasets
164 exist to robustly test this hypothesis.

165
166 The ‘time-stability’ of snow distribution on glaciers has particularly important
167 implications for long-term glacier mass balance programs, as seasonal and annual mass
168 balance solutions are derived from the integration of a limited number of point
169 observations (e.g., 3 to 50 stakes), and the assumption that stake and snow pit
170 observations accurately represent interannual variability in mass balance rather than
171 interannual variability in the spatial patterns of mass balance. Previous work has shown
172 ‘time-stability’ in the spatial pattern of annual mass balance (e.g., Vincent et al., 2017)
173 and while this is important for understanding the uncertainties in glacier-wide mass
174 balance estimates, the relative contributions of accumulation and ablation to this stability
175 are poorly constrained, thereby hindering a process-based understanding of these spatial
176 patterns. Furthermore, accurately quantifying the magnitude and spatial distribution of
177 winter snow accumulation on glaciers is a prerequisite for understanding the water budget
178 of glacierized basins, with direct implications for any potential use of this water, whether
179 that be ecological, agricultural, or human consumption (Kaser et al., 2010).

180

181 To better understand the ‘time-stability’ of the spatial pattern of snow accumulation on
182 glaciers, we present five consecutive years of extensive GPR observations for two
183 glaciers in Alaska. First, we use these GPR-derived SWE measurements to train two
184 different types of statistical models, which were subsequently used to spatially
185 extrapolate SWE across each glacier’s area. Second, we assess the temporal stability in
186 the resulting spatial distribution in SWE. Finally, we compare GPR-derived winter mass
187 balance estimates to traditional glaciological derived mass balance estimates and quantify
188 the uncertainty that interannual variability in spatial patterns in snow accumulation
189 introduces to these estimates.

190

191 **2. Study Area**

192 During the spring seasons of 2013–2017, we conducted GPR surveys on Wolverine and
193 Gulkana glaciers, located on the Kenai Peninsula and eastern Alaskan Range in Alaska
194 (Fig. 1). These glaciers have been studied as part of the U.S. Geological Survey’s
195 Benchmark Glacier project since 1966 (O’Neel et al., 2014). Both glaciers are ~16 km² in
196 area and span ~1200 m in elevation (426 – 1635 m asl for Wolverine, 1163 – 2430 m asl
197 for Gulkana). Wolverine Glacier exists in a maritime climate, characterized by warm air
198 temperatures (mean annual temperature = –0.2 °C at 990 meters; median equilibrium line
199 altitude for 2008 – 2017 is 1235 m asl) and high precipitation (median glacier-wide
200 winter balance = 2.0 m water equivalent (m w.e.)), while Gulkana is located in a
201 continental climate, characterized by colder air temperatures (mean annual temperature =
202 –2.8 °C at 1480 meters; median equilibrium line altitude for 2008 – 2017 is 1870 m asl)
203 and less precipitation (median glacier-wide winter balance = 1.2 m w.e.) (Fig. 2). The
204 cumulative mass balance time series for both glaciers is negative (~ –24 m w.e. between
205 1966–2016), with Gulkana showing a more monotonic decrease over the entire study
206 interval, while Wolverine exhibited near equilibrium balance between 1966 and 1987,
207 and sharply negative to present (O’Neel et al., 2014; O’Neel et al., 2018).

208

209 **3. Methods**

210 The primary SWE observations are derived from a GPR measurement of two-way travel
211 time (*twt*) through the annual snow accumulation layer. We describe five main steps to
212 convert *twt* along the survey profiles to annual distributed SWE products for each glacier.
213 These include (i) acquisition of GPR and ground-truth data, (ii) calculation of snow
214 density and associated radar velocity, which are used to convert measured *twt* to annual
215 layer depth and subsequently SWE, and (iii) application of terrain parameter statistical
216 models to extrapolate SWE across the glacier area. We then describe approaches to (iv)
217 evaluate the temporal consistency in spatial SWE patterns and (v) compare GPR-derived
218 SWE and direct (glaciological) winter mass balances.

219

220 3.1. Radar data collection and processing

221 Common-offset GPR surveys were conducted with a 500 MHz Sensors and Software
222 ~~pulseEkko Pro system in late spring close to maximum end-of-winter SWE and prior to~~
223 the onset of extensive surface melt. GPR parameters were set to a waveform-sampling
224 rate of 0.1 ns, a 200-ns time window, and “Free Run” trace increments, where samples
225 are collected as fast as the processor allows, instead of at uniform temporal or spatial
226 increments.

227

228 In general, GPR surveys were conducted by mounting a plastic sled behind a snowmobile
229 and driving at a near-constant velocity of 15 km h⁻¹ (Fig. 3, S1, S2), resulting in a trace
230 spacing of ~20 cm. Coincident GPS data were collected using a Novatel Smart-V1 GPS
231 receiver (Omnistar corrected, L1 receiver with root-mean-square accuracy of 0.9 m
232 (Perez-Ruiz et al., 2011)). We collected a consistent survey track from year-to-year that
233 minimized safety hazards (crevasses, avalanche runouts) but optimized the sampling of
234 terrain parameter space on the glacier (e.g., range and distribution of elevation, slope,
235 aspect, curvature, etc.). However, in 2016 at Wolverine Glacier, weather conditions and
236 logistics did not allow for ground surveys to be completed. Instead, a number of radar
237 lines were collected via a helicopter survey. To best approximate the ground surveys
238 completed in other years, we selected a subset of helicopter GPR observations within 150
239 m of the ground-based surveys. Previous comparisons between ground and helicopter

Deleted: P

Deleted:

242 platforms found excellent agreement in SWE point observations (coefficient of
243 determination (R^2)=0.96, root mean square error=0.14 m; McGrath et al., 2015).

244

245 Radargrams were processed using the ReflexW-2D software package (Sandmeier
246 Scientific Software). All radargrams were corrected to time zero, taken as the first
247 negative peak in the direct wave (Yelf and Yelf, 2006), and a dewow filter (mean
248 subtraction) was applied over 2 ns. When reflectors from the base of the seasonal snow
249 cover were insufficiently resolved, gain and band-pass filters were subsequently applied.
250 Layer picking was guided by ground-truth efforts and done semi-automatically using a
251 phase-following layer picker. For further details, please see McGrath et al. (2015).

252

253 **3.2. Ground truth observations**

254 We collected extensive ground-truth data to validate GPR surveys, including probing and
255 snowpit/cores. In the ablation zone of each glacier, we probed the snowpack thickness
256 every ~500 m along-track. In addition, we measured seasonal snow depth and density at
257 an average of five locations (corresponding to the glaciological observations; see Section
258 3.5) on each glacier in each year. Typically these locations include one or two in the
259 ablation zone, one near the long-term ELA, and two or more in the accumulation zone.
260 We measured snow density using a gravimetric approach in snowpits (at 10 cm intervals)
261 and with 7.25 cm diameter cores (if total depth >2 m; at 10–40 cm intervals depending on
262 natural breaks) to the previous summer surface. We calculated a density profile and
263 column-average density, ρ_{site} , at each site.

264

265 As snow densities did not exhibit a consistent spatial nor elevation dependency on the
266 glaciers (e.g., Fausto et al., 2018), we calculated a single average density, ρ , of all ρ_{site}
267 on each glacier and each year, which was subsequently used to calculate SWE:

268

$$269 \quad SWE = \left(\frac{twt}{2}\right) \cdot v_s \cdot \rho. \quad (1)$$

270

271 where twt is the two-way travel time as measured by the GPR and v_s is the radar
272 velocity. v_s was calculated for each glacier in each year as the average of two

273 independent approaches: (i) an empirical relationship based on the glacier-wide average ρ
274 (Kovacs et al., 1995) and (ii) a least-squares regression between snow depth derived by
275 probing and all radar *twt* observations within a 3-m radius of the probe site. An
276 exception was made at Wolverine in 2016 as no coincident probe depth observations
277 were made during the helicopter-based surveys. Instead, we estimated the second radar
278 velocity by averaging radar velocities calculated from observed *twt* and snow depths at
279 three snowpit/core locations.

280

281 **3.3. Spatial Extrapolation**

282 Extrapolating SWE from point measurements to the basin scale has been a topic of
283 focused research for decades (e.g., Woo and Marsh, 1978; Elder et al., 1995; Molotch et
284 al., 2005). Most commonly, the dependent variable SWE is related to a series of
285 explanatory terrain parameters, which are proxies for the physical processes that actually
286 control SWE distribution across the landscape. These include orographic gradient in
287 precipitation (elevation), wind redistribution of existing snow (slope, curvature, drift
288 potential), and aspect with respect to solar radiation and prevailing winds (eastness,
289 northness). We derived terrain parameters from 10-m resolution digital elevation models
290 (DEMs) sourced from the ArcticDEM project (Noh and Howat, 2015) for Gulkana and
291 produced from airborne Structure from Motion photogrammetry at Wolverine (Nolan et
292 al., 2015). Both DEMs were based on imagery from August 2015. Specifically, these
293 parameters include elevation, surface slope, surface curvature, northness (Molotch et al.,
294 2005), eastness, and snow drift potential (*Sb*) (Winstral et al., 2002; Winstral et al., 2013;
295 Fig. S3, S4). The *Sb* parameter is commonly used to identify locations where airflow
296 separation occurs based on both near and far-field topography and are thus likely
297 locations to accumulate snow drifts (Winstral et al., 2002). For specific details on this
298 calculation, please refer to Winstral et al. (2002). In the application of *Sb* here, we
299 determined the principle direction by calculating the modal daily wind direction during
300 the winter (October – May) when wind speeds exceeded 5 m s^{-1} (~minimum wind
301 velocity for snow transport; Li and Pomeroy, 1997). The length scales for curvature were
302 found using an optimization scheme that identified the highest model R^2 .

303

304 Prior to spatial extrapolation, we aggregated GPR observations to the resolution of the
305 DEM by calculating the median value of all observations within each 10 m pixel of the
306 DEM. We then utilized two approaches to extrapolate GPR point observations across the
307 glacier surface: (i) least-squares elevation gradient applied to glacier hypsometry and (ii)
308 statistical models. For (i), we derived SWE elevation gradients in two ways; first, solely
309 on observations that followed the glacier centerline and second, from the entire spatially-
310 extensive dataset. For (ii), we utilized ~~two different models~~: stepwise multivariable linear
311 regressions and regression trees (Breiman et al., 1984). All of these approaches produced
312 a spatially-distributed SWE field over the entire glacier area. Individual points in this
313 field are equivalent to point winter balances (b_w ; m w.e.). From the distributed b_w field,
314 we calculated a mean area-averaged winter balance (B_w ; m w.e.).

Deleted: both

316 Additionally, we implemented a cross-validation approach to the statistical ~~models~~
317 (multivariable regression and regression tree), whereby 75 % of the aggregated
318 observations were used for training and 25 % were used for testing. However, rather than
319 randomly selecting pixels from across the entire dataset, we randomly selected a single
320 pixel containing aggregated GPR observations and then extended this selection out along
321 continuous survey lines until we reached 25 % of the total observational dataset, thus
322 removing entire sections (and respective terrain parameters) from the analysis (Fig. S5).
323 This approach provided a more realistic test for the statistical models, as the random
324 selection of individual cells did not significantly alter terrain-parameter distributions. For
325 each glacier and each year, we produced 100 training/test dataset combinations, but rather
326 than take the single model with the highest R^2 or lowest RMSE (~~between modelled SWE~~
327 ~~and the GPR-derived test dataset~~), we produced a distributed SWE product by taking the
328 median value for each pixel from all 100 model runs and a glacier-wide median value
329 that is the median of all 100 individual B_w estimates. We chose the median-value
330 approach over a highest R^2 /lowest RMSE approach that is often utilized because, despite
331 being randomly selected, some training datasets were inherently advantaged by a more
332 complete ~~sampling of terrain parameter distributions~~. These iterations resulted in the
333 highest R^2 /lowest RMSE when applied to the training dataset, but weren't necessarily

Deleted: extrapolations

Deleted: from the resulting

Deleted:

Deleted: test dataset

Deleted: distribution of

Deleted:

Deleted: s

342 indicative of a better model, particularly in the context of being able to predict SWE at
343 locations on the glacier where the terrain parameter space had not been well sampled.

Deleted: .

344 3.3.2. Stepwise Multivariable Linear Regression

345 We used a stepwise multivariable linear regression model of the form,

$$346 SWE_{(i,j)} = c_1x_{1(i,j)} + c_2x_{2(i,j)} + \dots + c_nx_{n(i,j)} + \varepsilon_{(i,j)}, \quad (2)$$

347 where $SWE_{(i,j)}$ is the predicted (standardized) value at location i,j and c_1, c_2, c_n are the beta
348 coefficients of the model, x_1, x_2, x_n are terrain parameters which are independent variables
349 that have been standardized and ε is the residual. We applied the regression model
350 stepwise and included an independent variable if it minimized the Akaike information
351 criterion (AIC; Akaike, 1974). We present the beta coefficients from each regression
352 (each year, each glacier) to explore the temporal stability of these terms.

353 3.3.3. Regression Trees

354 Regression trees (Breiman et al., 1984) provide an alternative statistical approach for
355 extrapolating point observations by recursively partitioning SWE into progressively more
356 homogenous subsets based on independent terrain parameter predictors (Molotch et al.,
357 2005; Meromy et al., 2013; Bair et al., 2018). The primary advantage of the regression
358 tree approach is that each terrain parameter is used multiple times to partition the
359 observations, thereby allowing for non-linear interactions between these terms. In
360 contrast, the MVR only allows for a single “global” linear relationship for each parameter
361 across the entire parameter-space. We implemented a random forest approach (Breiman,
362 2001) of repeated regression trees (100 learning cycles) in Matlab, using weak learners
363 and bootstrap aggregating (bagging; Breiman, 1996). Each weak learner omits 37% of
364 observations, such that these “out-of-bag” observations are used to calculate predictor
365 importance. The use of this ensemble/bagging approach reduces overfitting and thus
366 precludes having to subjectively prune the tree and provides more accurate and unbiased
367 error estimates (Breiman, 2001). Prior to implementing the regression tree, we removed
368 the SWE elevation gradient from the observations using a least-squares regression. As
369 described in the results, elevation is the dominant independent variable and as our
370 observations (particularly at Wolverine) did not cover the entire elevation range, the
371
372

374 regression tree approach was not well suited to predicting SWE at elevations outside of
375 the observational range.

376

377 **3.4. Interannual variability in spatial patterns**

378 We quantified the stability of spatial patterns in SWE across the five-year interval using
379 two approaches: (i) normalized range and (ii) the coefficient of determination. In the first
380 approach, we first divided each pixel in the distributed SWE fields by the glacier-wide
381 average, B_w , for each year and each glacier, and then calculated the range in these

382 normalized values over the entire five-year interval. For example, if a cell had normalized
383 values of 84 %, 92 %, 106 %, 112 % and 120 %, the normalized range would be 36 %. A
384 limitation of this approach is that it is highly sensitive to outliers, such that a single year
385 can substantially increase this range. This is similar to an approach presented by Sold et
386 al. (2016), but unlike their calculation (their Fig. 9), the normalized values reported here
387 have not been further normalized by the normalized mean of that pixel over the study
388 interval. Thus, the values reported here are an absolute normalized range, whereas Sold et
389 al. (2016) report a relative normalized range. In the coefficient of determination (R^2)
390 approach, we computed the least-squares regression correlation between the SWE in each
391 pixel and the glacier-wide average, B_w , derived from the MVR model over the five-year
392 period. For this approach, cells with a higher R^2 scale linearly with the glacier-wide
393 average, while those with low R^2 do not.

394

395 **3.5. Glaciological mass balance**

396 Beginning in 1966, glacier-wide seasonal (winter, B_w ; summer, B_s) and annual balances (B_a)
397 were derived from glaciological measurements made at three fixed locations on each glacier.
398 The integration of these point measurements was accomplished using a site-index method –
399 equivalent to an area-weighted average (March and Trabant, 1996; van Beusekom et al., 2010).
400 Beginning in 2009, a more extensive stake network of seven to nine stakes was established on
401 each glacier, thereby facilitating the use of a balance profile method for spatial extrapolation
402 (Cogley et al., 2011). Systematic bias in the glaciological mass balance time-series is removed
403 via a geodetic adjustment derived from DEM differencing over decadal timescales (e.g.,
404 O’Neel et al., 2014). For this study, glaciological measurements were made within a day of the

Deleted: has

406 GPR surveys, and integrated over the glacier hypsometry using both the historically applied
407 site-index method (based on the long-term three stake network) and the more commonly
408 applied balance profile method (based on the more extensive stake network). We utilized a
409 single glacier hypsometry, derived from the 2015 DEMs, for each glacier over the entire five-
410 year interval. Importantly, in order to facilitate a more direct comparison to the GPR-derived
411 B_w estimates, we used glaciological B_w estimates that have not been geodetically calibrated.

412

413 **4. Results**

414 **4.1. General accumulation conditions**

415 Since 1966, Wolverine Glacier's median B_w (determined from the stake network) exceeds
416 Gulkana's by more than a factor of two (2.3 vs. 1.1 m w.e.), and exhibits greater
417 variability, with an interquartile range more than twice as large (0.95 m w.e. vs. 0.4 m
418 w.e.). Over the five-year study period, both glaciers experienced accumulation conditions
419 that spanned their historical ranges, with one year in the upper quartile (including the 5th
420 greatest B_w at Wolverine in 2016), one year within 25% of the median, and multiple years
421 in the lower quartile (2017 at Gulkana and 2014 at Wolverine had particularly low B_w
422 values) (Fig. 2). In all years, B_w at Wolverine was greater, although in 2013 and 2014, the
423 difference was only 0.1 m w.e.

424

425 Average accumulation season (taken as October 1 – May 31) wind speeds over the study
426 period were stronger ($\sim 7 \text{ m s}^{-1}$ vs. $\sim 3 \text{ m s}^{-1}$) and from a more consistent direction at
427 Wolverine than Gulkana (northeast at Wolverine, southwest to northeast at Gulkana)
428 (Fig. S6). On average, Wolverine experienced ~ 50 days with wind gusts $> 15 \text{ m s}^{-1}$ each
429 winter, while for Gulkana, this only occurred on ~ 7 days. Over the five-year study period,
430 interannual variability in wind direction was very low at Wolverine (2016 saw slightly
431 greater variability, with an increase in easterly winds). In contrast, at Gulkana, winds
432 were primarily from the northeast to east in 2013–2015, from the southwest to south in
433 2016–2017, and experienced much greater variability during any single winter.

434

435 **4.2. *In situ* and GPR point observations**

436 Glacier-averaged snow densities across all years were 440 kg m^{-3} (range $414\text{--}456 \text{ kg m}^{-3}$) at Wolverine and 362 kg m^{-3} (range $328\text{--}380 \text{ kg m}^{-3}$) at Gulkana (Table S1). Average
437 radar velocities were 0.218 m ns^{-1} (range $0.207\text{--}0.229 \text{ m ns}^{-1}$) at Wolverine and 0.223 m ns^{-1} ($0.211\text{--}0.231 \text{ m ns}^{-1}$) at Gulkana. Over this five-year interval, the GPR point
438 observations revealed a general pattern of increasing SWE with elevation, along with
439 fine-scale variability due to wind redistribution (e.g., upper elevations of Wolverine) and
440 localized avalanche input (e.g., lower west branch of Gulkana) (Fig. S1, S2). The
441 accumulation season (hereafter, winter) SWE elevation gradient was steeper (~ 440 vs.
442 $\sim 115 \text{ mm } 100 \text{ m}^{-1}$) and more variable in its magnitude at Wolverine than Gulkana.
443 Gradients ranged between $348\text{--}624 \text{ mm } 100 \text{ m}^{-1}$ at Wolverine, and $74\text{--}154 \text{ mm } 100 \text{ m}^{-1}$ at Gulkana (Fig. 4). Over all five years at both glaciers, elevation explained between 50
444 % and 83 % of the observed variability in SWE (Fig. 4).

448

449 4.3. Model performance

450 To evaluate model performance in unsampled locations of the glacier, both extrapolation
451 approaches were run 100 times for each glacier and each year, each time with a unique,
452 randomly selected training (75 % of aggregated observations) and test (remaining 25 %
453 of aggregated observations) dataset. The median and standard deviation of the
454 coefficients of determination (R^2) ~~between modeled SWE and the test datasets for the 100~~
455 models runs are shown in Fig. 5. Model performance ranged from 0.25 to 0.75, but on
456 average, across both glaciers and all years, was 0.56 for the MVR approach and 0.46 for
457 the regression tree. Model performance was higher and more consistent at Wolverine,
458 whereas 2015 and 2017 at Gulkana had test dataset R^2 of ~ 0.4 and 0.3, likely reflecting
459 the lower winter SWE elevation gradients and coefficients of determination with
460 elevation during these years (Fig. 4). The wide range in R^2 across the 100 model runs
461 reflects the variability in training and test datasets that were randomly selected. When the
462 test dataset terrain parameter space was captured by the training dataset, a high
463 coefficient of determination resulted, but when the test dataset terrain parameter space
464 was exclusive (e.g., contained only a small elevation range), the model performance was
465 typically low. This further highlights the importance of elevation as a predictor for these
466 glaciers.

Deleted: from these

Deleted: .

Deleted: .

470
471 At Gulkana, the model residuals (Fig. S1) exhibited spatiotemporal consistency, with
472 positive residuals (i.e., observed SWE exceeded modeled SWE by ~ 0.2 m w.e.) at mid-
473 elevations of the west branch, and at the very terminus of the glacier. The largest negative
474 residuals typically occurred at the highest elevations. In both cases, these locations
475 deviated from the overall SWE elevation gradient. At Wolverine, observations at the
476 highest elevations typically exceeded the modeled SWE (i.e., positive residuals),
477 particularly at the highest elevations of the northeast corner where wind drifting is
478 particularly prevalent (Fig. S2). For example, in 2015, nearly 80% of the residuals in this
479 section were positive and had a median value of 0.4 m. Elsewhere at Wolverine, the
480 residuals often alternated between positive and negative values over length scales of 10s
481 to 100s of meters (Fig. S2), which we interpret as zones of scour/drift not captured by the
482 MVR model.

Deleted: in the northeast quadrant of the glacier

Deleted: that were better captured by the regression tree models.

483
484 The beta coefficients of terrain parameters from the MVR were fairly consistent from
485 year-to-year at both glaciers (Fig. 6). At Wolverine, elevation was the largest beta
486 coefficient, followed by Sb and curvature. At Gulkana, elevation was also the largest beta
487 coefficient, followed by curvature. Gulkana experiences much greater variability in wind
488 direction during the winter months (Fig. S6), possibly explaining why Sb was either not
489 included or had a very low beta coefficient in the median regression model. As our
490 surveys were completed prior to the onset of ablation, terrain parameters related to solar
491 radiation gain (notably the terms that include aspect: northness and eastness) had small
492 and variable beta coefficients.

493 494 **4.4. Spatial Variability**

495 A common approach for quantifying snow accumulation variability across a range of
496 means is the coefficient of variation (CoV), which is calculated as the ratio of the
497 standard deviation to the mean (Liston et al., 2004; Winstral and Marks, 2014). The mean
498 and standard deviation of CoVs at Wolverine were 0.42 ± 0.03 and at Gulkana, $0.29 \pm$
499 0.05 , indicating relatively lower spatial variability in SWE at Gulkana (Fig. 7). CoVs
500 were fairly consistent across all five years, although 2017 saw the largest CoVs at both

504 glaciers. Interestingly, 2017 had the lowest absolute spatial variability (i.e., lowest
505 standard deviation), but also the lowest glacier-wide averages during the study period,
506 resulting in greater CoVs.

507

508 Qualitatively, both Wolverine and Gulkana glaciers exhibited consistent spatiotemporal
509 patterns in accumulation across the glacier surface, with elevation exerting a first-order
510 control (Fig. 8, S7, S8). Overlaid on the strong elevational gradient are consistent
511 locations of wind scour and deposition, reflecting the interaction of wind redistribution
512 and complex – albeit relatively stable year to year – surface topography (consisting of
513 both land and ice topography). For instance, numerous large drifts (~2 m amplitude, ~200
514 m wavelength) occupy the northeast **and northwest** corners of Wolverine Glacier, where
515 prevailing northeasterly winds consistently redistributed snow into sheltered locations in
516 each year of the study period (Fig. 8). The different statistical extrapolation approaches
517 produced nearly identical B_w estimates (4 % difference on average at Wolverine and 1 %
518 difference on average at Gulkana) (Fig. 9). The MVR B_w estimate was larger in 4 out of 5
519 years at Wolverine (Fig. 9), while neither approach exhibited a consistent bias at
520 Gulkana.

521

522 Although the glacier-wide averages between these approaches showed close agreement,
523 we explored the differences in spatial patterns by calculating a mean SWE difference
524 map for each glacier by differencing the five-year mean SWE produced by the regression
525 tree model from the same produced by the MVR model (Fig. 10). As such, locations
526 where the MVR exceeded the regression tree are positive (yellow). At Gulkana, where
527 the two approaches showed slightly better glacier-wide B_w agreement, the magnitude in
528 individual pixel differences were substantially less than at Wolverine (e.g., color bar
529 scales range ± 0.2 m at Gulkana vs. ± 0.5 m at Wolverine). At Wolverine Glacier, there
530 were three distinct elevation bands where the MVR approach predicted greater SWE,
531 namely the main icefall in the ablation zone, a region of complex topography centered
532 around a normalized elevation of 0.65, and lastly, at higher elevations, where both
533 approaches predicted a series of drift and scour zones, although in sum, the MVR model
534 predicted greater SWE.

535

536 We used two different approaches to quantify the ‘time-stability’ of spatial patterns
537 across these glaciers. By the first metric, normalized range, we found that both glaciers
538 exhibited very similar patterns (Fig. 11), with either ~65 or 85 % (regression tree and
539 MVR, respectively) of the glacier area experiencing less than 25 % absolute normalized
540 variability (Fig. 12). The R^2 approach provides an alternative way of assessing the time
541 stability of SWE, essentially determining whether SWE at each location scales with the
542 glacier-wide value. By this metric, 80 % of the glacier area at Wolverine and 96 % of the
543 glacier area at Gulkana (based on MVR model) had a coefficient of determination greater
544 than 0.8 (Fig. 12), suggesting that most locations on the glacier have a consistent
545 relationship with the mean glacier-wide mass balance. By both metrics, the MVR output
546 suggests greater ‘time-stability’ (e.g., lower normalized range or higher R^2) compared to
547 the regression tree.

548

549 **4.5. Winter mass balance**

550 In order to examine systematic variations between the approaches we outlined in Section
551 3 for calculating the glacier-wide winter balance, B_w , we first calculated a yearly mean
552 from the six approaches (including four based on the GPR observations: MVR,
553 regression tree, elevation gradient derived from centerline only observations, elevation
554 gradient derived from all point observations, and two based on the *in situ* stake network:
555 site-index and profile). In general, Gulkana exhibited greater agreement (4 % average
556 difference) among the approaches, with most approaches agreeing within 5 % of the six-
557 approach mean (Fig. 13; Table S2). Wolverine showed slightly less agreement (7 %
558 average difference), as the two terrain parameters statistical extrapolations (MVR and
559 regression tree) produced B_w estimates ~9 % above the mean, while the two stake derived
560 estimates were ~7 % less than the mean. On average across all five years at Wolverine,
561 the MVR approach was the most positive, while the glaciological site-index approach
562 was always the most negative (Fig. 13). At both glaciers, the estimates using elevation as
563 the only predictor yielded B_w estimates on average within 3 % of the six-method mean,
564 with the centerline only based estimate being slightly negatively biased, and the complete
565 observations being slightly positively biased.

566

567 To examine the systematic difference between the glaciological site-index method and
568 GPR-based MVR approach, we compared stake-derived b_w values from the three long-
569 term stakes to all GPR-based MVR b_w values within that index zone (Fig. 14). Both the
570 stakes and the GPR-derived b_w values have been normalized by the glacier-wide value to
571 make these results comparable across years and glaciers. It is apparent that Wolverine
572 experienced much greater spatial variability in accumulation, with larger interquartile
573 ranges and a large number of positive outliers in all index zones. Importantly, the stake
574 weight in the site-index solution is dependent on the hypsometry of the glacier, and for
575 both glaciers, the upper stake accounts for ~65 % of the weighted average. In years that
576 the misfit between GPR B_w and site-index B_w was largest (2015 and 2016 at Gulkana,
577 2013 and 2017 at Wolverine), the stake-derived b_w at the upper stake was in the lower
578 quartile of all GPR-derived b_w values, explaining the significant difference in B_w
579 estimates in these years. Potential reasons for this discrepancy are discussed in Section
580 5.3.

581

582 *In situ* stake and pit observations traditionally serve as the primary tool for deriving
583 glaciological mass balances. However, in order for these observations to provide a
584 systematic and meaningful long-term record, they need to record interannual variability
585 in mass balance rather than interannual variability in spatial patterns of mass balance. To
586 assess the performance of the long-term stake sites, we examined the interannual
587 variability metrics for the stake locations. By both metrics (normalized absolute range
588 and R^2), the middle and upper elevation stakes at both glaciers appear to be in locations
589 that achieve this temporal stability, having exhibited ~10 % range and $R^2 > 0.95$ over the
590 five-year interval. The lower elevation stake was less temporally stable and exhibited
591 opposing behavior at each glacier. At Gulkana, this stake had a high R^2 (0.93) and
592 moderate normalized variability (26 %), which in part, reflects the lower total
593 accumulation at this site and the ability for a single uncharacteristic storm to alter this
594 total amount significantly. In contrast, Wolverine's lowest site exhibited both low R^2
595 (< 0.01) and normalized range (2 %), a somewhat unlikely combination. The statistical
596 models commonly predicted zero or near-zero cumulative winter accumulation at this site

Deleted: spatial

Deleted: in

Deleted: extrapolation approaches frequently

600 (i.e., mid-winter rain and/or ablation is common at this site), so although the normalized
601 range was quite low, predicted SWE values were uncorrelated with B_w over the study
602 interval.

603

604 **Discussion**

605 **5.1. Interannual variability in spatial patterns**

606 Each glacier exhibited consistent normalized SWE spatial patterns across the five-year
607 study, reflecting the strong control of elevation and regular patterns in wind redistribution
608 in this complex topography (Fig. 11, S7, S8). This is particularly notable given the highly
609 variable magnitudes of accumulation over the five-year study and the contrasting climate
610 regions of these two glaciers (wet, warm maritime and cold, dry continental), with unique
611 storm paths, timing of annual accumulation, wind direction and wind direction
612 variability, and snow density. At both glaciers, the lowest interannual variability was
613 found away from locations with complex topography and elevated surface roughness,
614 such as crevassed zones, glacier margins, and areas near peaks and ridges.

615

616 In the most directly comparable study using repeat GPR surveys at Switzerland's
617 Findelgletscher, 86 % of the glacier area experienced less than 25 % range in relative
618 normalized accumulation over a three-year interval (Sold et al., 2016). As noted in
619 Section 3.4., we reported an absolute normalized range, whereas Sold et al. (2016)
620 reported a relative normalized range. Following their calculation, we found that 81 and
621 82 % of Wolverine and Gulkana's area experienced a relative normalized range less than
622 25 %. Collectively, our results add to the growing body of evidence (e.g., Deems et al.,
623 2008; Sturm and Wagner, 2010; Schirmer et al., 2011; Winstral and Marks, 2014)
624 suggesting 'time-stability' in the spatial distribution of snow in locations that span a
625 range of climate zones, topographic complexity, and relief. While the initial effort
626 required to constrain the spatial distribution over a given area can be significant, the
627 benefits of understanding the spatial distribution are substantial and long-lasting, and
628 have a wide range of applications.

629

630 **5.1.1 Elevation**

631 Elevation explained between 50 and 83 % of the observed SWE variability at Gulkana
632 and Wolverine, making it the most significant terrain parameter at both glaciers every
633 year (Fig. 4, 6). Steep winter SWE gradients characterized both glaciers throughout the
634 study period (115 – 440 mm 100 m⁻¹). Such gradients are comparable to previous results
635 for glaciers in the region (Pelto, 2008; Pelto et al., 2013; McGrath et al., 2015), but
636 exceed reported orographic precipitation gradients in other mountainous regions by a
637 factor of 2–3 (e.g., Anderson et al., 2014; Grünewald and Lehning, 2011). These steep
638 gradients are likely the result of physical processes beyond just orographic precipitation,
639 including storm systems that deliver snow at upper elevations and rain at lower elevations
640 (common at both Wolverine and Gulkana) and mid-winter ablation at lower elevations (at
641 Wolverine). These processes have also been shown to steepen observed SWE gradients
642 relative to orographic precipitation gradients in a mid-latitude seasonal snow watershed
643 (Anderson et al., 2014). Unfortunately, given that we solely sampled snow distribution at
644 the end of the accumulation season, the relative magnitude of each of these secondary
645 processes is not constrained.

646
647 Wolverine and Gulkana glaciers exhibited opposing SWE gradients at their highest
648 elevations, with Wolverine showing a sharp non-linear increase in SWE, while Gulkana
649 showed a gradual decrease. This non-linear increase was also noted at two maritime
650 glaciers (Scott and Valdez) in 2013 (McGrath et al., 2015), and perhaps reflects an
651 abundance of split precipitation phase storms in these warm coastal regions. The cause of
652 the observed reverse gradient at Gulkana may be the result of wind scouring at the
653 highest and most exposed sections of the glacier, or in part, a result of where we were
654 able to safely sample the glacier. For instance, in 2013, when we were able to access the
655 highest basin on the glacier, the SWE elevation gradient remained positive (Fig. 4).
656 Reductions in accumulated SWE at the highest elevations have also been observed at
657 Lemon Creek Glacier in southeast Alaska and Findel Glacier in Switzerland (Machguth
658 et al., 2006), presumably related to wind scouring at these exposed elevations.

659

660 **5.1.2. Wind redistribution**

661 Both statistical extrapolation approaches found terrain parameters S_b and curvature,
662 proxies for wind redistribution, to have the largest beta coefficients after elevation (Fig.
663 6, S9). The spatial pattern of SWE estimated by each model clearly reflects the dominant
664 influence of wind redistribution and elevation (Fig. 8), as areas of drift and scour are
665 apparent, especially at higher elevations. However, these terms do not fully capture the
666 redistribution process, as the model residuals (Fig. S1, S2) show sequential positive and
667 negative residuals associated with drift/scour zones. There are a number of reasons why
668 this might occur, including variable wind directions transporting snow (this is likely a
669 more significant issue at Gulkana, which experiences greater wind direction variability
670 (Fig. S6)), complex wind fields that are not well represented by a singular wind direction
671 (Dadic et al., 2010), changing surface topography (the glacier surface is dynamic over a
672 range of temporal scales, changing through both surface mass balance processes and ice
673 dynamics), and widely varying wind velocities. This is particularly relevant at Wolverine,
674 where wind speeds regularly gust over 30 m s^{-1} during winter storms, speeds that result in
675 variable length scales of redistribution that would not be captured by a fixed length scale
676 of redistribution. All of these factors influence the redistribution of snow and limit the
677 predictive ability of relatively simple proxies. Significant effort has gone into developing
678 physically-based snow-distribution models (e.g., Alpine3D and SnowModel), however,
679 high-resolution meteorological forcing data requirements generally limit the application
680 of these models in glacierized basins. Where such observations do exist, previous studies
681 have illuminated how the final distribution of snow is strongly correlated to the complex
682 wind field, including vertical (surface normal) winds (Dadic et al., 2010).

683

684 **5.1.3. Differences with non-glaciated terrain**

685 Although our GPR surveys did not regularly include non-glaciated regions of these
686 basins, a few key differences are worth noting. First, the length scales of variability on
687 and off the glacier were distinctly different, with shorter scales and greater absolute
688 variability (snow-free to $>5 \text{ m}$ in less than 10 m distance) off-glacier (Fig. S10). This
689 point has been clearly shown using airborne LiDAR in a glaciated catchment in the
690 Austrian Alps (Helfricht et al., 2014). The reduced variability on the glacier is largely due
691 to surface mass balance and ice flow processes that act to smooth the surface, leading to a

692 more spatially consistent surface topography, and therefore a more spatially consistent
693 SWE pattern. For this reason, establishing a SWE elevation gradient on a glacier is likely
694 much less prone to terrain-induced outliers compared to off-glacier sites, although the
695 relationship of this gradient to off-glacier gradients is generally unknown.

696

697 **5.2. Spatial differences between statistical models**

698 The two statistical extrapolation approaches yielded comparable large-scale spatial
699 distributions and glacier-wide averages, although there were some notable spatial
700 differences (Fig. 10). The systematic positive bias of the MVR approach over the
701 regression tree at Wolverine was due to three sectors of the glacier with both complex
702 terrain (i.e., icefalls) and large data gaps (typically locations that are not safe to access on
703 ground surveys). The difference in predicted SWE in these locations is likely due to how
704 the two statistical extrapolation approaches handle unsampled terrain parameter space.
705 The MVR extrapolates based on global linear trends, while the regression tree assigns
706 SWE from terrain that most closely resembles the under-sampled location. Anecdotally,
707 it appears that the MVR may overestimate SWE in some of these locations, which is most
708 evident in Wolverine's lower icefall, where bare ice is frequently exposed at the end of
709 the accumulation season (Fig. S11) in locations where the MVR predicted substantial
710 SWE. Likewise, the regression tree models could be underestimating SWE in these
711 regions, but in the absence of direct observations the errors are inherently unknown. The
712 regression tree model captures more short length scale variability while the MVR model
713 clarifies the larger trends. Consequently, smaller drifts and scours are captured well by
714 the regression tree model in areas where the terrain parameter space is well surveyed, but
715 the results become progressively less plausible as the terrain becomes distinctly different
716 from the sampled terrain parameter space. In contrast, the MVR model appears to give
717 more plausible results at larger spatial scales. This suggests that there is some theoretical
718 threshold where the regression tree is more appropriate if the terrain parameter space is
719 sampled sufficiently, but that for many glacier surveys the MVR model would be more
720 appropriate.

721

722 **5.3. Winter mass balance comparisons**

Deleted: more

724 On average, all methods for estimating B_w were within $\pm 11\%$ of the six-method mean,
725 (Fig. 13). The agreement (as measured by the average percent difference from the mean)
726 between estimates was slightly better at Gulkana than Wolverine, likely reflecting the
727 overall lower spatial variability at Gulkana and the greater percentage of the glacier area
728 where b_w correlates well with the glacier-wide average (Fig. 11 e, f). At both glaciers, B_w
729 solutions based solely on elevation showed excellent agreement to the six-method mean,
730 suggesting that this simple approach is a viable means for measuring B_w on these glaciers.
731 The biggest differences occurred between the GPR-forced MVR model and the
732 glaciological site-index method, which we've shown is attributed to the upper stake (with
733 the greatest weight) underestimating the median SWE for that index zone (Fig. 14). The
734 upper stake location was established in 1966 at an elevation below the median elevation
735 of that index zone, which given the strong elevation control on SWE, is a likely reason
736 for the observed difference. At Gulkana, the relationship between the upper index site
737 and the GPR-forced MVR model is more variable in large part due to observed
738 differences in the accumulation between the main branch (containing the index site) and
739 the west branch of the glacier (containing additional stakes added in 2009). Such basin-
740 scale differences are likely present on many glaciers with complex geometry, and thus
741 illustrate potential uncertainties of using a small network of stakes to monitor the mass
742 balance of these glaciers. In the context of the MVR model, this manifests as a change in
743 sign in the eastness coefficient (which separates the branches in parameter space; Fig.
744 S4). Notably, in the two years where the site-index estimate was most negatively biased
745 at Gulkana (2015 and 2016), the glaciological profile method, relying on the more
746 extensive stake network (which includes stakes in the west branch of the glacier), yielded
747 B_w estimates within a few percent of the GPR-derived MVR estimate.

748

749 These GPR-derived B_w results have important implications for the cumulative
750 glaciological (stake-derived) mass balance time-series (currently only based on the site-
751 index method), which is calibrated with geodetic observations ([details on the site-index](#)
752 [method and geodetic calibrations can be found in Van Beusekom et al., 2010 and O'Neel](#)
753 [et al., 2014](#)). It is important to remember that the previous comparisons (e.g., Fig. 13)
754 were based on glaciological B_w values that have not had a geodetic calibration applied. At

755 Wolverine, the cumulative annual glaciological mass balance solutions are positively
756 biased compared to the geodetic mass balance solutions over decadal timescales,
757 requiring a negative calibration ($-0.43 \text{ m w.e. a}^{-1}$; O’Neel et al., 2014) to be applied to
758 the glaciological solutions. The source of this disagreement is some combination of the
759 stake-derived winter and summer balances being too positive relative to the geodetic
760 solution. On average, the GPR-derived B_w results were $\sim 0.4 \text{ m w.e.}$ more positive than the
761 site-index B_w results at Wolverine, which would further increase the glaciological-
762 geodetic solution difference and suggest that the stake-derived glaciological solutions are
763 underestimating ablation (B_s) by $\sim 0.8 \text{ m w.e. a}^{-1}$. Preliminary observations at Wolverine
764 using ablation wires show that some sectors of the glacier experience very high ablation
765 rates that are not captured by the stake network (e.g., crevassed zones through enhanced
766 shortwave solar radiation gain (e.g., Pfeffer and Bretherton, 1987; Cathles et al., 2011;
767 Colgan et al., 2016), and/or increased turbulent heat fluxes due to enhanced surface
768 roughness), and/or ice margins (through enhanced longwave radiation from nearby snow-
769 free land cover)). However, these results are not universal, as the assimilation of
770 distributed GPR observations at Findelgletcher significantly improved the comparison
771 between geodetic and modeled mass balance estimates (Sold et al., 2016), suggesting
772 multiple drivers of glaciologic-geodetic mismatch for long-term mass balance programs.

773

774 **5.3.1. Implications for stake placement**

775 Understanding the spatiotemporal distribution of SWE is useful for informing stake
776 placements and also for quantifying the uncertainty that interannual spatial variations in
777 SWE introduce to historic estimates of glacier-wide mass balance, particularly when
778 long-term mass balance programs rely on limited numbers of point observations (e.g.,
779 USGS and National Park Service glacier monitoring programs; O’Neel et al., 2014;
780 Burrows, 2014). Our winter balance results illustrate that stakes placed at the same
781 elevation are not directly comparable, and hence are not necessarily interchangeable in
782 the context of a multi-year mass balance record. Most locations on the glacier exhibit bias
783 from the average mass balance at that elevation and our results suggest interannual
784 consistency in this bias over sub-decadal time scales. As a result, constructing a balance

785 profile using a small number of inconsistently located stakes is likely to introduce large
786 relative errors from one year to the next.

787

788 Considering this finding, the placement of stakes to measure snow accumulation is
789 dependent on whether a single glacier-wide winter mass balance value (B_w) or a spatially
790 distributed SWE field is desired as a final product. For the former, a small number of
791 stakes can be distributed over the glacier hypsometry in areas where interannual
792 variability is low. Alternatively, if a distributed field is desired, a large number of stakes
793 can be widely distributed across the glacier, including areas where the interannual
794 variability is higher. In both cases it is important to have consistent locations from year to
795 year, although as the number of stakes increases significantly, this becomes less critical.

796

797 We assess the uncertainty that interannual variability in the spatial distribution of SWE
798 introduces to the historic index-method (March and Trabant, 1996) mass balance
799 solutions by first calculating the uncertainty, σ , contributed by each stake as:

800
$$\sigma_{stake} = \sigma_{model\ residuals} + (1 - R^2) \cdot u, \quad (3)$$

801 where $\sigma_{model\ residuals}$ is the standard deviation of MVR model residuals over all five
802 years within ± 30 meters of the index site, u is the mean b_w within ± 30 meters of the
803 index site, and R^2 is the coefficient of determination between b_w and B_w over the five-year
804 period (Fig. 11). The first term on the right hand side of Eq. 3 accounts for both the
805 spatial and temporal variability in the observed b_w as compared to the model, and the
806 second term accounts for the variability of the model as compared to B_w . The glacier-
807 wide uncertainty from interannual variability is then:

808
$$Glacier\ \sigma = \sqrt{\sum_{all\ stakes} (\sigma_{stake} \cdot w_{stake})^2}, \quad (4)$$

809 where w_{stake} is the weight function from the site-index method (which depends on stake
810 location and glacier hypsometry). By this assessment, interannual variability in the spatial
811 distribution of SWE at stake locations introduced minor uncertainty, on the order of 0.11
812 m w.e. at both glaciers (4 % and 10 % of B_w at Wolverine and Gulkana, respectively).

813 This suggests that the original stake network design at the benchmark glaciers does
814 remarkably well at capturing the interannual variability in glacier-wide winter balance.

815 The greatest interannual variability at each glacier is found at the lowest stake sites, but

816 because b_w and the stake weights are both quite low at these sites, they contribute only
817 modestly to the overall uncertainty. Instead, the middle and upper elevation stakes
818 contribute the greatest amount to the glacier-wide uncertainty.

Deleted: slightly

819

820 **6. Conclusions**

821 We collected spatially extensive GPR observations at two glaciers in Alaska for five
822 consecutive winters to quantify the spatiotemporal distribution of SWE. We found good
823 agreement of glacier-average winter balances, B_w , among the four different approaches
824 used to extrapolate GPR point measurements of SWE across the glacier hypsometry.
825 Extrapolations relying only on elevation (i.e., a simple balance profile) produced B_w
826 estimates similar to the more complicated statistical models, suggesting that this is an
827 appropriate method for quantifying glacier-wide winter balances at these glaciers. The
828 more complicated approaches, which allow SWE to vary across a range of terrain-
829 parameters based on DEMs, show a high degree of temporal stability in the pattern of
830 accumulation at both glaciers, as ~85 % of the area on both glaciers experienced less than
831 25 % normalized absolute variability over the five-year interval. Elevation and the
832 parameters related to wind redistribution had the most explanatory power, and were
833 temporally consistent at each site. The choice between MVR and regression tree models
834 should depend on both the range in terrain parameter space that exists on the glacier,
835 along with how well that space is surveyed.

Deleted: -

836

837 In total, six different methods (four based on GPR measurements and two based on stake
838 measurements) for estimating the glacier-wide average agreed within ± 11 %. The site-
839 index glaciological B_w estimates were negatively biased compared to all other estimates,
840 particularly when the upper-elevation stake significantly underestimated SWE in that
841 index zone. In contrast, the profile glaciological approach, using a more extensive stake
842 network, showed better agreement with the other approaches, highlighting the benefits of
843 using a more extensive stake network.

844

845 We found the spatial patterns of snow accumulation to be temporally stable on these
846 glaciers, which is consistent with a growing body of literature documenting similar

849 consistency in a wide variety of environments. The long-term stake locations experienced
850 low interannual variability in normalized SWE, meaning that stake measurements tracked
851 the interannual variability in SWE, rather than interannual variability in spatial patterns.
852 The uncertainty associated with interannual spatial variability is only 4–10 % of the
853 glacier-wide B_w at each glacier. Thus, our findings support the concept that sparse stake
854 networks can be effectively used to measure interannual variability in winter balance on
855 glaciers.

856

857 *Data Availability.* The GPR and associated observational data used in this study can be
858 accessed on the USGS Glaciers and Climate Project website
859 (<https://doi.org/10.5066/F7M043G7>). The Benchmark Glacier mass balance input and
860 output can be accessed at: <https://doi.org/10.5066/F7HD7SRF> (O’Neel et al., 2018). The
861 Gulkana DEM is available from the ArcticDEM project website
862 (<https://www.pgc.umn.edu/data/arcticdem/>) and the Wolverine DEM is available at
863 <ftp://bering.gps.alaska.edu/pub/chris/wolverine/>. A generalized version of the SWE
864 extrapolation code is available at: [https://github.com/danielmcgrathCSU/Snow-](https://github.com/danielmcgrathCSU/Snow-Distribution)
865 [Distribution](https://github.com/danielmcgrathCSU/Snow-Distribution).

866

867 *Author Contributions.* SO, DM, LS, and HPM designed the study. DM performed the
868 analyses and wrote the manuscript. LS contributed to the design and implementation of
869 the analyses, and CM, SC, and EHB contributed specific components of the analyses. All
870 authors provided feedback and edited the manuscript.

871

872 *Competing Interests.* The authors declare that they have no conflict of interest.

873

874 *Acknowledgments.* This work was funded by the U.S. Geological Survey Land Change
875 Science Program, USGS Alaska Climate Adaptation Science Center, and DOI/USGS
876 award G17AC00438 to DM. Any use of trade, firm, or product names is for descriptive
877 purposes only and does not imply endorsement by the U.S. Government. We
878 acknowledge the Polar Geospatial Center (NSF-OPP awards 1043681, 1559691, and
879 1542736) for the Gulkana DEM. We thank Caitlyn Florentine, Jeremy Littell, Mauri

880 Pelto, and an anonymous reviewer for their thoughtful feedback that improved the
881 manuscript.

882

883 **References**

884

885 Akaike, H.: A new look at the statistical model identification, *IEEE Trans. Autom.*
886 *Control*, AC-19(6), 1974.

887

888 Anderson, B. T., McNamara, J. P., Marshal, H. P., and Flores, A. N.: Insights into the
889 physical processes controlling correlations between snow distribution and terrain
890 properties, *Water Res. Res.*, 50(6), 4545–4563, doi:10.1002/2013WR013714, 2014.

891

892 Bauder, A. (ed): *The Swis Glaciers, 2013/14 and 2014/15*, Glaciological Report (Glacier)
893 No. 135/136, doi:10.18752/glrep_135-136, 2017.

894

895 Bair, E. H., Calfa, A.A., Rittger, K., and Dozier, J.: Using machine learning for real-time
896 estimates of snow water equivalent in the watersheds of Afghanistan, *The Cryosphere*,
897 12, 1579–1594, doi:10.5194/tc-12-1579-2018, 2018.

898

899 Balk, B. and Elder, K.: Combining binary regression tree and geostatistical methods to
900 estimate snow distribution in a mountain watershed, *Water Res. Res.*, 36(1), 13–26, 2000.

901

902 [Beamer, J.P., Hill, D.F., McGrath, D., Arendet, A., and Kienholz, C.: Hydrologic impacts](#)
903 [of changes in climate and glacier extent in the Gulf of Alaska watershed, *Water Res.*](#)
904 [Res., 53, doi:10.1002/2016WR020033.](#)

905

906 Burrows, R.: Annual report on vital signs monitoring of glaciers in the Central Alaska
907 Network 2011–2013, Natural Resource Technical Report NPS/CAKN/NRTR—2014/905,
908 National Park Service, Fort Collins, Colorado, 2014.

909

910 Breiman, L.: Bagging predictors, *Mach. Learn.*, 24, 123–140,
911 <https://doi.org/10.1023/A:1018054314350>, 1996.

912

913 Breiman, L.: Random forests, *Mach. Learn.*, 45, 5–32,
914 <https://doi.org/10.1023/A:1010933404324>, 2001.
915
916 Breiman, L., Friedman, J. H., Olshen, R. A., and Stone, C. J.: Classification and
917 Regression Trees, Chapman and Hall, New York, 368 pp., 1984.
918
919 Cathles, L. C., Abbot, S. D., Bassis, J. N., and MacAyeal, D.R.: Modeling surface-
920 roughness/solar-ablation feedback: application to small-scale surface channels and
921 crevasses of the Greenland ice sheet, *Ann. Glaciol.*, 52(59), 99–108, 2011.
922
923 Cogley, J. G., Hock, R., Rasmussen, L. A., Arendt, A. A., Bauder, A., Braithwaite, R. J.,
924 Jansson, P., Kaser, G., Möller, M., Nicholson, L. and Zemp, M.: Glossary of Glacier
925 Mass Balance and Related Terms, IHP-VII Technical Documents in Hydrology No. 86,
926 IACS Contribution No. 2, UNESCO-IHP, Paris, 2011.
927
928 Colgan, W., Rajaram, H., Abdalati, W., McCutchan, C., Mottram, R., Moussavi, M. S.,
929 and Grigsby, S.: Glacier crevasses: Observations, models, and mass balance implications,
930 *Rev. Geophys.*, 54, doi:10.1002/2015RG000504, 2016.
931
932 Dadic, R., Mott, R., Lehning, M., and Burlando, P.: Wind influence on snow depth
933 distribution and accumulation over glaciers, *J. Geophys. Res.*, 115, F01012,
934 doi:10.1029/2009JF001261, 2010.
935
936 Deems, J. S., Fassnacht, S. R., and Elder, K. J.: Interannual consistency in fractal snow
937 depth patterns at two Colorado mountain sites, *J. Hydromet.*, 9, 977–988,
938 doi:10.1175/2008JHM901.1, 2008.
939
940 Elder, K., Michaelsen, J., and Dozier, J.: Small basin modeling of snow water
941 equivalence using binary regression tree methods, *IAHS Publ.* 228, 129–139, 1995.
942

943 Erickson, T. A., Williams, M.W., and Winstral, A.: Persistence of topographic controls
944 on the spatial distribution of snow in rugged mountain terrain, Colorado, United States,
945 *Water Res. Res.*, 41, W04014, doi:10.129/2003WR002973, 2005.

946

947 Escher-Vetter, H., Kuhn, M., and Weber, M.: Four decades of winter mass balance of
948 Vernagtferner and Hintereisferner, Austria: methodology and results, *Ann. Glaciol.*,
949 50(50), 2009.

950 Fausto, R.S., and 11 others.: A Snow Density Dataset for Improving Surface Boundary
951 Conditions in Greenland Ice Sheet Firm Modeling, *Front. Earth Sci.*, 6(51),
952 doi:10.3389/feart.2018.00051, 2018.

953 Fitzpatrick, N., Radić, V., and Menounos, B.: Surface energy balance closure and
954 turbulent flux parameterization on a mid-latitude mountain glacier, Purcell Mountains,
955 Canada, *Front. Earth Sci.*, 5(67), doi:10.3389/feart.2017.00067, 2017.

956 Grünewald, T., and Lehning, M.: Altitudinal dependency of snow amounts in two alpine
957 catchments: Can catchment-wide snow amounts be estimated via single snow or
958 precipitation stations?, *Ann. Glaciol.*, 52(58), 153–158, 2011.

959 Helfricht, K., Schöber, J., Schneider, K., Sailer, R., and Kuhn, M.: Interannual
960 persistence of the seasonal snow cover in a glacierized catchment, *J. Glaciol.*, 60(223),
961 doi:10.3189/2014JoG13J197, 2014.

962

963 Hock, R.: Glacier melt: a review of processes and their modeling, *Prog. Phys. Geog.*, 29,
964 362–391, doi:10.1191/0309133305pp453ra, 2005.

965

966 Hock, R., Hutchings, J. K., and Lehning, M.: Grand challenges in cryospheric sciences:
967 toward better predictability of glaciers, snow and sea ice, *Front. Earth Sci.*, 5(64),
968 doi:10.3389/feart.2017.00064, 2017.

969

970 Hodgkins, R., Cooper, R., Wadham, J., and Tranter, M.: Interannual variability in the
971 spatial distribution of winter accumulation at a high-Arctic glacier (Finstervaldereen,
972 Svalbard), and its relationship with topography, *Ann. Glaciol.*, 42, 243–248, 2005.
973
974 Huss, M. and Hock, R.: A new model for global glacier change and sea-level rise, *Front.*
975 *Earth Sci.*, 3, doi:10.3389/feart.2015.00054, 2015.
976 Kaser, G., Großhauser, M., and Marzeion, B.: Contribution potential of glaciers to water
977 availability in different climate regimes, *Proc. Natl. Acad. Sci.*, 107, 20,223–20,227,
978 doi:10.1073/pnas.1008162107, 2010.
979
980 Klos, P. Z., Link, T. E., and Abatzoglou, J. T.: Extent of the rain-snow transition zone in
981 the western U.S. under historic and projected climate, *Geophys. Res. Lett.*, 41, 4560–
982 4568, doi: 10.1002/2014GL060500, 2014.
983
984 Kovacs, A., Gow, A. J., and Morey, R. M.: The in-situ dielectric constant of polar firn
985 revisited, *Cold Reg. Sci. Tech.*, 23, 245–256, 1995.
986
987 Kuhn, M.: The mass balance of very small glaciers, *Z. Gletscherkd. Glazialgeol.*, 31(1–
988 2), 171–179, 1995.
989
990 Lehning, M., Grünewald, T., and Schirmer, M.: Mountain snow distribution governed by
991 altitudinal gradient and terrain roughness, *Geophys. Res. Lett.*, 38, L19504,
992 doi:10.1029/2011GL048927, 2011.
993
994 Li, L. and Pomeroy, J. W.: Estimates of threshold wind speeds for snow transport using
995 meteorological data, *J. Applied Met.*, 36, 205-213, 1997.
996
997 Liston, G. E., and Elder, K.: A distributed snow-evolution modeling system
998 (SnowModel), *J. Hydromet.*, 7, 1259-1276, 2006.
999

Deleted: [Knowles, N., Dettinger, M. D., and Cayan, D. R.: Trends in snowfall versus rainfall in the Western United States, *J. Climate*, 19, 4545–4559, 2006.](#)

1004 Littel, J. S., McAfee, S. A., and Hayward, G. D.: Alaska snowpack response to climate
1005 change: statewide snowfall equivalent and snowpack water scenarios, *Water*, 10 (5), doi:
1006 10.3390/w10050668, 2018.
1007
1008 Kjølmoen, B. (ed), Andreassen L.M., Elvehøy, H., Jackson, M., and Melvold, J:
1009 Glaciological investigations in Norway 2016, NVE Rapport 76 2017, 108 pp, 2017.
1010
1011 Marks, D., Domingo, J., Susong, D., Link, T., and Garen, D.: A spatially distributed
1012 energy balance snowmelt model for application in mountain basins, *Hydrol. Processes*,
1013 13, 1935–1959, 1999.
1014
1015 Machguth, H., Eisen, O., Paul, F., and Hoelzle, M.: Strong spatial variability of snow
1016 accumulation observed with helicopter-borne GPR on two adjacent Alpine glaciers,
1017 *Geophys. Res. Lett.*, 33, L13503, doi:10.1029/2006GL026576, 2006.
1018
1019 March, R. S., and Trabant, D. C.: Mass balance, meteorological, ice motion, surface
1020 altitude, and runoff data at Gulkana Glacier, Alaska, 1992 balance year, *Water-Resources*
1021 *Investigations Report*, 95-4277, 1996.
1022
1023 McAfee, S., Walsh, J., and Rupp, T. S.: Statistically downscaled projections of snow/rain
1024 partitioning for Alaska, *Hydrol. Process.*, 28(12), 3930–3946, doi:10.1002/hyp.9934,
1025 2013.
1026
1027 McGrath, D., Sass, L., O’Neel, S., Arendt, A., Wolken, G., Gusmeroli, A., Kienholz, C.,
1028 and McNeil, C.: End-of-winter snow depth variability on glaciers in Alaska, *J. Geophys.*
1029 *Res. Earth Surf.*, 120, 1530–1550, doi:10.1002/2015JF003539, 2015.
1030
1031 McGrath, D., Sass, L., O’Neel, S., Arendt, A. and Kienholz, C.: Hypsometric control on
1032 glacier mass balance sensitivity in Alaska and northwest Canada, *Earth’s Future*, 5, 324–
1033 336, doi:10.1002/2016EF000479, 2017.
1034

1035 Meromy, L., Molotch, N. P., Link, T. E., Fassnacht, S. R., and Rice, R.: Subgrid
1036 variability of snow water equivalent at operational snow stations in the western USA,
1037 Hydro. Proc., 27, 2383-2400, doi:10.1002/hyp.9355, 2013.
1038
1039 Molotch, N. P., Colee, M. T., Bales, R. C. and Dozier, J.: Estimating the spatial
1040 distribution of snow water equivalent in an alpine basin using binary regression tree
1041 models: the impact of digital elevation data and independent variable selection, Hydrol.
1042 Proc., 19, 1459–14-79, doi:10.1002/hyp.5586, 2005.
1043
1044 Nolan, M., Larsen, C., and Sturm, M.: Mapping snow depth from manned aircraft on
1045 landscape scales at centimeter resolution using structure-from-motion photogrammetry,
1046 The Cryosphere, 9, 1445-1463, doi:10.5194/tc-9-1445-2015, 2015.
1047
1048 Noh, M. J. and Howat, I. M.: Automated stereo-photogrammetric DEM generation at
1049 high latitudes: Surface Extraction with TIN-based Search-space Minimization (SETSM)
1050 validation and demonstration over glaciated regions, GIScience & Remote
1051 Sensing, 52(2), 198-217, doi:10.1080/15481603.2015.1008621, 2015.
1052
1053 O’Neel, S., Hood, E., Arendt, A., and Sass, L.: Assessing streamflow sensitivity to
1054 variations in glacier mass balance, Climatic Change, 123(2), 329–341,
1055 doi:10.1007/s10584-013-1042-7, 2014.
1056
1057 O’Neel, S., Fagre, D. B., Baker, E. H., Sass, L. C., McNeil, C. J., Peitzsch, E. H.,
1058 McGrath, D. and Florentine, C. E.: Glacier-Wide Mass Balance and Input Data: USGS
1059 Benchmark Glaciers, 1966-2016 (ver. 2.1, May 2018), U.S. Geological Survey data
1060 release, <https://doi.org/10.5066/F7HD7SRE>, 2018.
1061
1062 Painter, T., Berisford, D., Boardman, J., Bormann, K., Deems, J., Gehrke, F., Hedrick,
1063 A., Joyce, M., Laidlaw, R., Marks, D., Mattmann, C., McGurk, B., Ramirez, P.,
1064 Richardson, M., Skiles, S.M., Seidel, F., and Winstral, A.: The Airborne Snow
1065 Observatory: fusion of scanning lidar, imaging spectrometer, and physically-based

1066 modeling for mapping snow water equivalent and snow albedo, *Remote Sens. Environ.*,
1067 184, 139–152, doi:10.1016/j.rse.2016.06.018, 2016.
1068
1069 Pelto, M.: Utility of late summer transient snowline migration rate on Taku Glacier,
1070 Alaska, *The Cryosphere*, 5, 1127–1133, doi:10.5194/tc-5-1127-2011, 2011.
1071
1072 Pelto, M., Kavanaugh, J., and McNeil, C.: Juneau Icefield Mass Balance Program
1073 1946–2011, *Earth Syst. Sci. Data*, 5, 319–330, [https://doi.org/10.5194/essd-5-319-](https://doi.org/10.5194/essd-5-319-2013)
1074 2013, 2013.
1075
1076 Pérez-Ruiz, M., Carballido, J., and Agüera, J.: Assessing GNSS correction signals for
1077 assisted guidance systems in agricultural vehicles, *Precision Agric.*, 12, 639–652,
1078 doi:10.1007/s11119-010-9211-4, 2011.
1079
1080 Pfeffer, W. T., and Bretherton, C.: The effect of crevasses on the solar heating of a
1081 glacier surface, *IAHS Publ.*, 170, 191–205, 1987.
1082
1083 Pfeffer, W. T., et al.: The Randolph Glacier Inventory: A globally complete inventory of
1084 glaciers, *J. Glaciol.*, 60(221), 537–552, doi:10.3189/2014JoG13J176, 2014.
1085
1086 Schirmer, M., Wirz, V., Clifton, A., and Lehning, M.: Persistence in intra-annual snow
1087 depth distribution: 1. Measurements and topographic control, *Water Resour. Res.*, 47,
1088 W09516, doi:10.1029/2010WR009426, 2011.
1089
1090 Sold, L., Huss, M., Hoelzle, M., Anderegg, H., Joerg, P., and Zemp, M.:
1091 Methodological approaches to infer end-of-winter snow distribution on alpine glaciers, *J.*
1092 *Glaciol.*, 59(218), 1047–1059, doi:10.3189/2013JoG13J015, 2013.
1093
1094 Sold, L., Huss, M., Machguth, H., Joerg, P. C., Vieli, G. L., Linsbauer, A., Salzmann, N.,
1095 Zemp, M. and Hoelzle, M.: Mass balance re-analysis of Findelengletscher, Switzerland;

1096 Benefits of extensive snow accumulation measurements, *Front. Earth Sci.*, 4(18),
1097 doi:10.3389/feart.2016.00018, 2016.
1098
1099 Sturm, M. and Wagner, A. M.: Using repeated patterns in snow distribution modeling:
1100 An Arctic example, *Water Res. Res.*, 46 (12), doi:10.1029.2010WR009434, 2010.
1101
1102 Van Beusekom, A. E., O’Neel, S., March, R. S., Sass, L., and Cox, L. H.: Re-analysis of
1103 Alaskan Benchmark Glacier mass balance data using the index method, U.S. Geological
1104 Survey Scientific Investigations Report 2010–5247, 16 p., 2010.

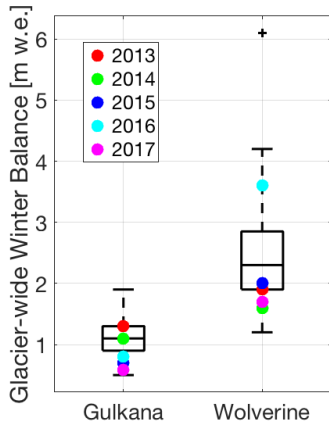
1105 Vincent, C., Fischer, A., Mayer, C., Bauder, A., Galos, S.P., Funk, M., Thibert, E., Six,
1106 D., Braun, L., and Huss, M.: Common climatic signal from glaciers in the European Alps
1107 over the last 50 years, *Geophys. Res. Lett.*, 44, 1376–1383, doi:10.1002/2016GL072094,
1108 2017.
1109
1110 Winstral, A., Elder, K., and Davis, R. E.: Spatial snow modeling of wind-redistributed
1111 snow using terrain-based parameters, *J. Hydrometeo.*, 3, 524–538, 2002.
1112
1113 Winstral, A., Marks, D. and Gurney, R.: Simulating wind-affected snow accumulations at
1114 catchment to basin scales, *Adv. Water Res.*, 55, 64–79,
1115 doi:10.1016/j.advwatres.2012.08.011, 2013.
1116
1117 Winstral, A. and Marks, D.: Long-term snow distribution observations in a mountain
1118 catchment: Assessing variability, time stability, and the representativeness of an index
1119 site, *Water Res. Res.*, 50, 293–305, doi:1002/2012WR013038, 2014.
1120
1121 Woo, M.-K., and Marsh, P.: Analysis of error in the determination of snow storage for
1122 small high Arctic basins, *J. Appl. Meteorol.*, 17, 1537–1541, 1978.
1123
1124 Yelf, R. and Yelf, D.: Where is true time zero?, *Electro. Phenom.*, 7(1), 158–163, 2006.
1125
1126

1127 Figure 1. Map of southern Alaska with study glaciers marked by red outline. All glaciers
1128 in the region are shown in white (Pfeffer et al., 2014).



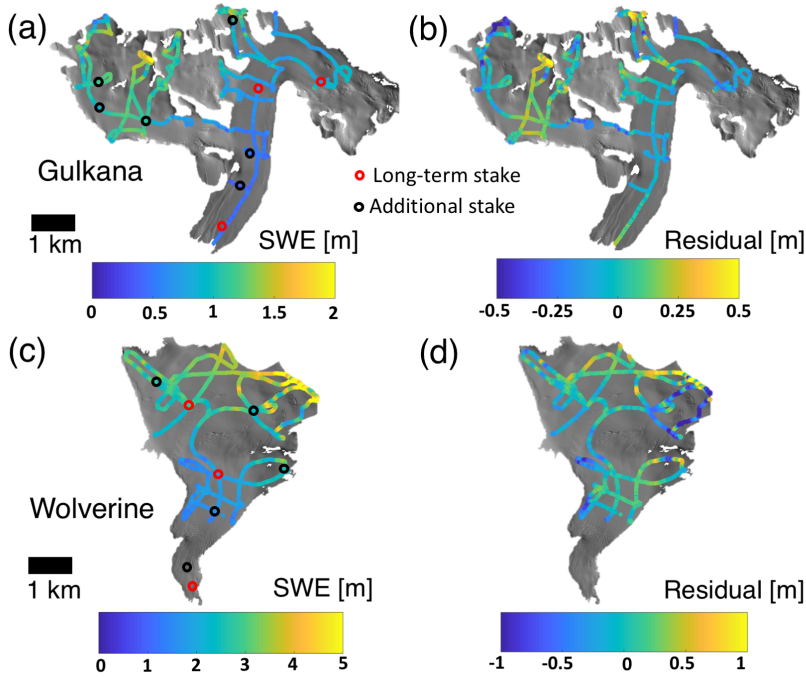
1129
1130
1131
1132
1133

1134 Figure 2. Boxplots of glacier-wide winter balance for Gulkana and Wolverine glaciers
1135 between 1966 and 2017. Years corresponding to GPR surveys are shown with colored
1136 markers. These values have not been adjusted by the geodetic calibration (see O'Neel et
1137 al., 2014).



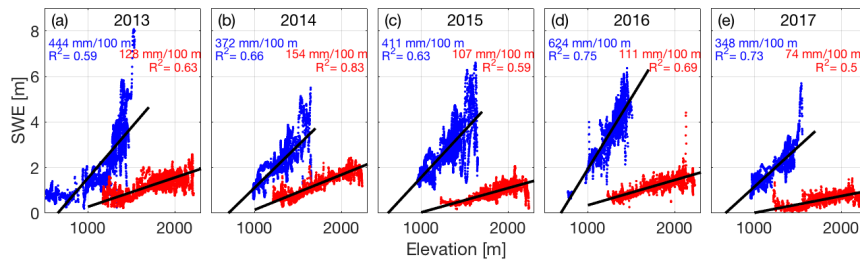
1138
1139
1140
1141

1142 Figure 3. GPR surveys from 2015 at Gulkana (a) and Wolverine (c) glaciers and MVR
 1143 model residuals (b, d).



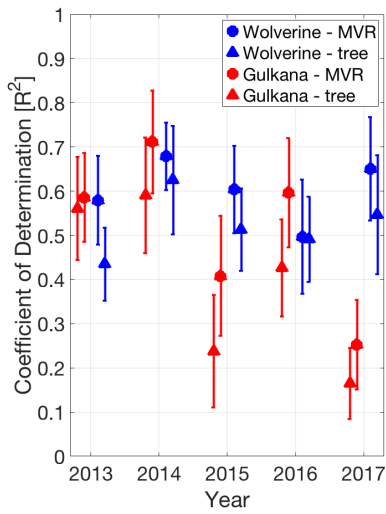
1144
 1145
 1146
 1147
 1148
 1149

Figure 4. SWE from GPR surveys as a function of elevation, along with least squares regression slope and coefficient of determination for each year of the study period. Wolverine is plotted in blue, Gulkana in red.



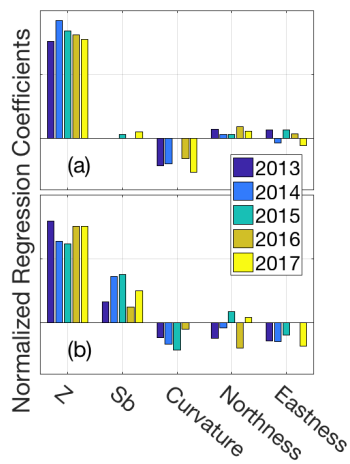
1150
 1151

1152 Figure 5. Median and standard deviation (error bars) of coefficient of determination
 1153 (from 100 model runs) for both extrapolation approaches (circles are MVR, triangles are
 1154 regression tree) developed on training datasets and applied to test datasets. Symbols and
 1155 error bars are offset from year for clarity.



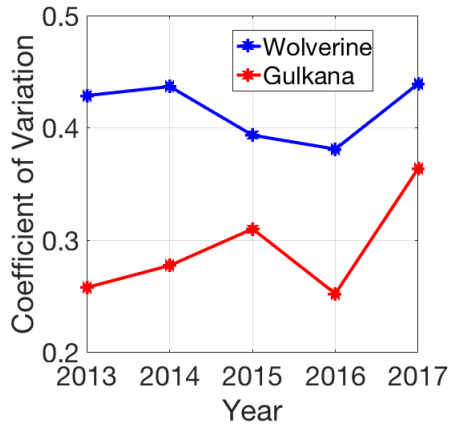
11 / 3

1174 Figure 6. Terrain parameter beta coefficients for (a) Gulkana and (b) Wolverine for
 1175 multivariable linear regression for each year of the study interval.



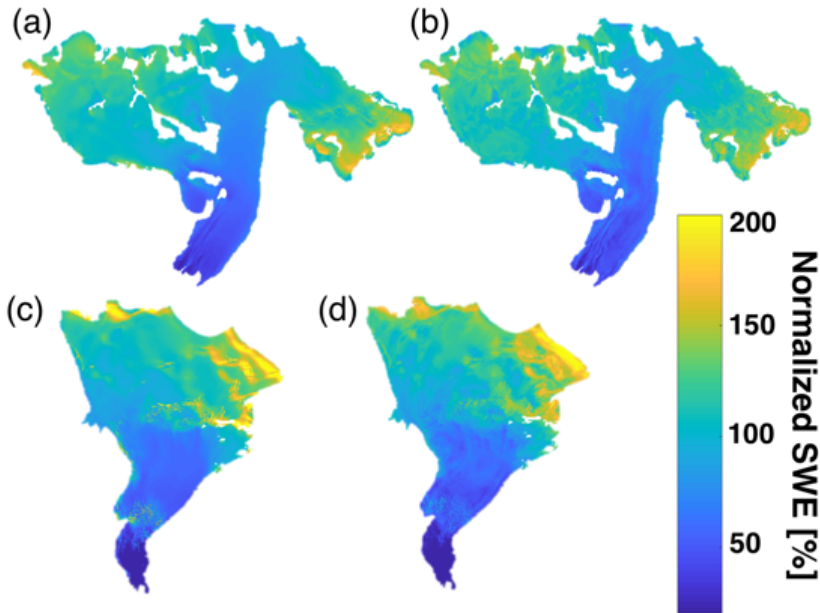
1176

1177 Figure 7. Spatial variability in snow accumulation across the glacier quantified by the
1178 coefficient of variation (standard deviation/mean) for each glacier across the five-year
1179 interval based on MVR model output.
1180



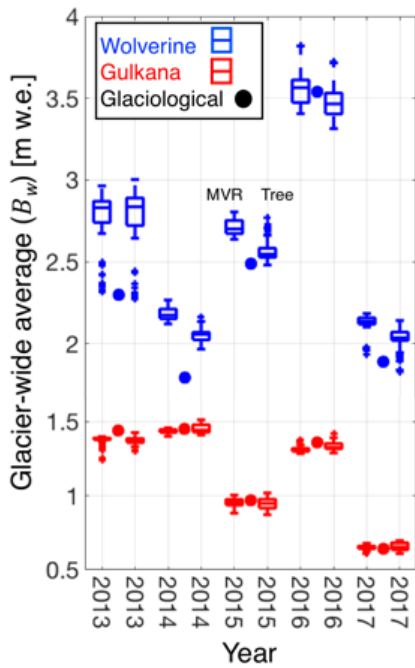
1181
1182

1183 Figure 8. Five-year mean of normalized distributed SWE for Gulkana (a,b) and
1184 Wolverine (c,d) for multivariable regression (a,c) and regression tree (b,d).



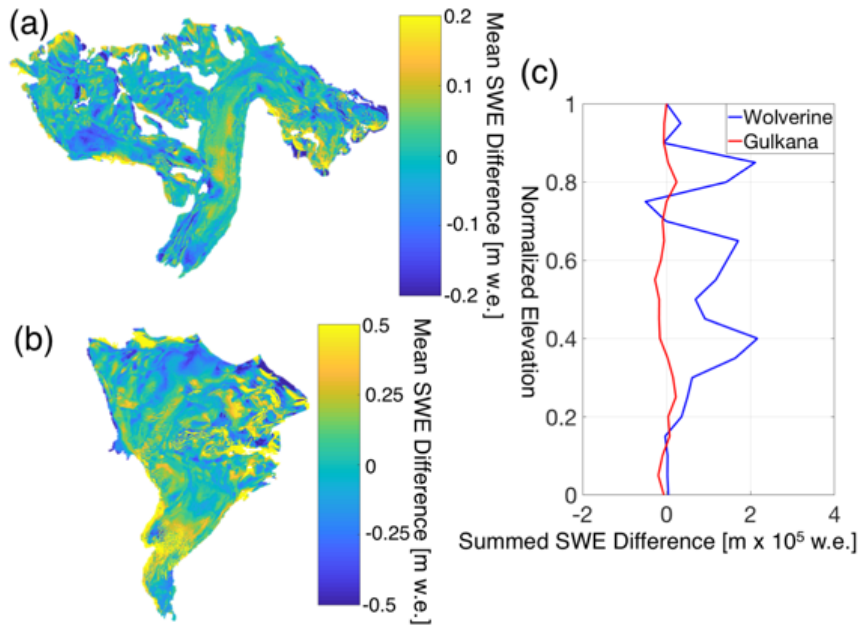
1185

1186 Figure 9. Comparing statistical models for GPR-derived glacier-wide winter balances for
 1187 both Wolverine (blue) and Gulkana (red) glaciers. For each year and each glacier, two
 1188 boxplots are shown. The first shows multivariable regression model (MVR) output and
 1189 the second shows regression tree output (tree). The B_w estimate from the glaciological
 1190 profile method is shown for each year and glacier as the filled circle.
 1191



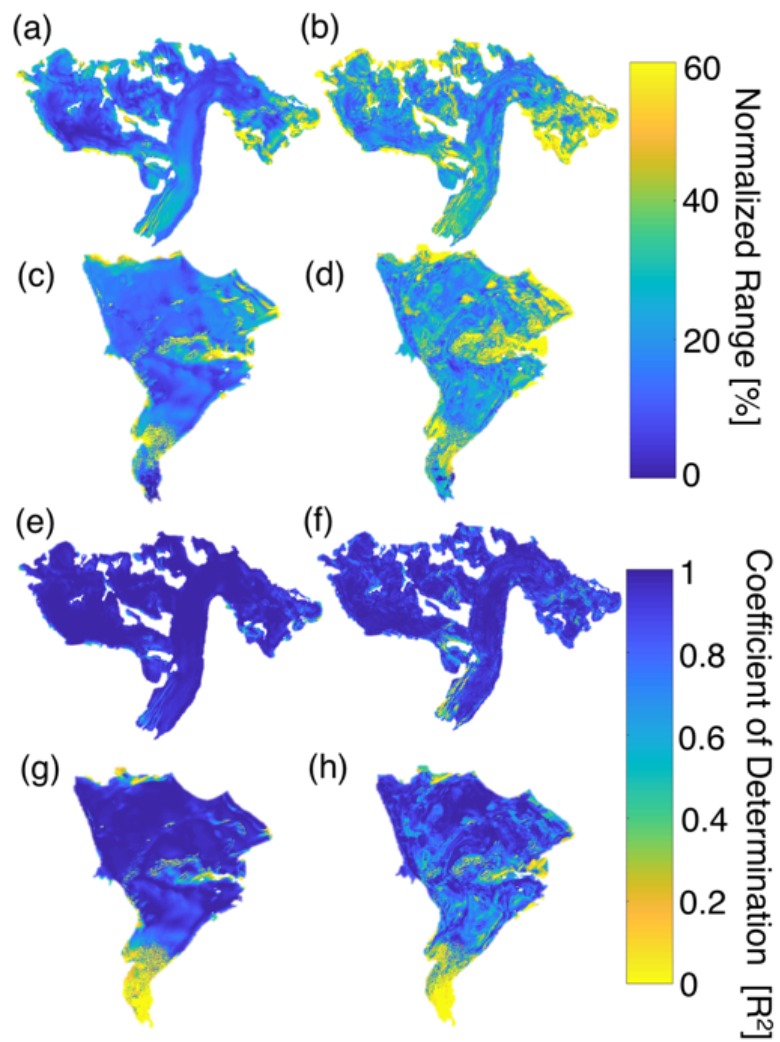
1192
 1193
 1194
 1195
 1196
 1197
 1198
 1199
 1200
 1201
 1202

1203 Figure 10. SWE differences between statistical models for Gulkana (a) and Wolverine
1204 (b) calculated by differencing the regression tree five-year mean SWE from the
1205 multivariable regression (MVR) five-year mean SWE. Yellow colors indicate regions
1206 where MVR yields more SWE than decision tree and blue colors indicate the opposite.
1207 Note different magnitude colorbar scales. c) Summed SWE difference between methods
1208 in bins of 0.05 normalized elevation values.



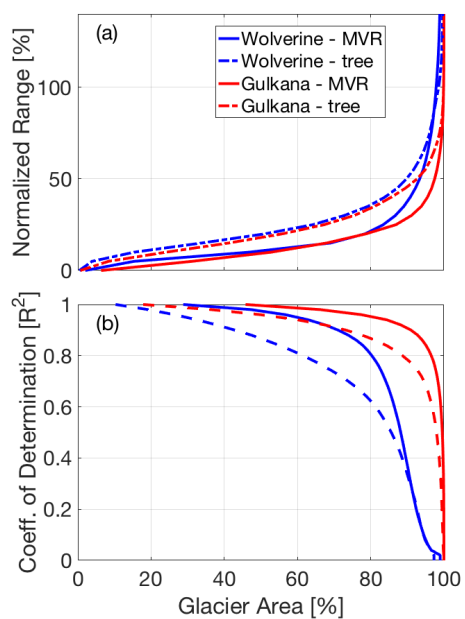
1209
1210
1211
1212
1213
1214
1215
1216
1217
1218
1219
1220
1221
1222

1223 Figure 11. Interannual variability of the SWE accumulation field from 2013–2017,
1224 quantified via normalized range (a-d) and R^2 (e-h) approach for median distributed fields
1225 from the multivariable regression (left column) and regression tree (right column)
1226 statistical models.



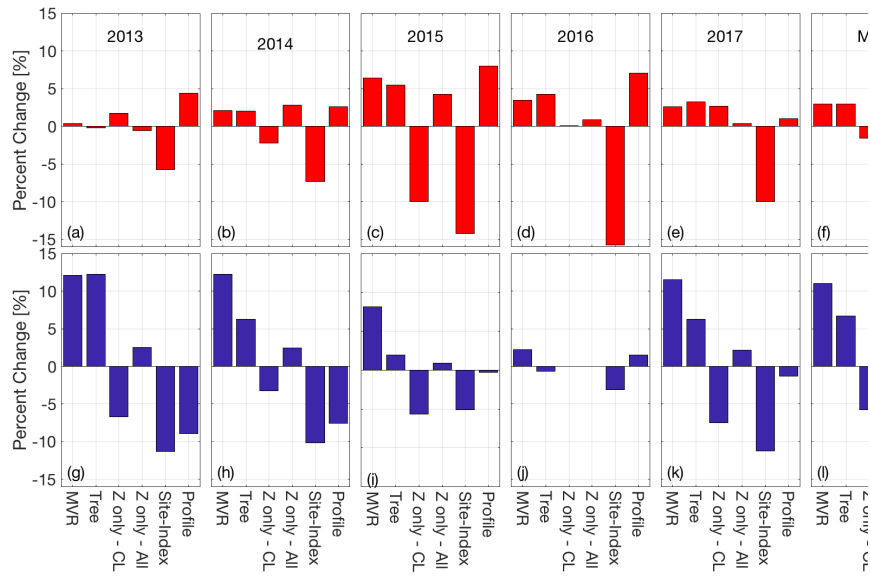
1227
1228

1229 Figure 12. Interannual variability of the SWE accumulation pattern as a function of
1230 cumulative glacier area, shown as (a) normalized range and (b) and R^2 . Solid lines are for
1231 multivariable regression (MVR) and dashed lines are regression tree.
1232



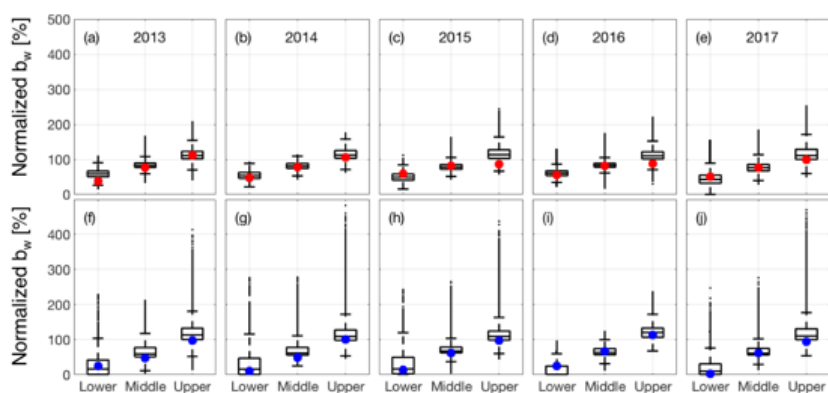
1233
1234
1235
1236
1237
1238
1239
1240
1241
1242
1243
1244
1245
1246
1247

1248 Figure 13. Percent deviation for each estimate from the six-method mean of B_{yr} .
 1249 Individual years for Gulkana Glacier are shown in panels a-e with the five-year mean
 1250 shown in f. Individual years for Wolverine Glacier are shown in panels g-k, with the five-
 1251 year mean shown in l.



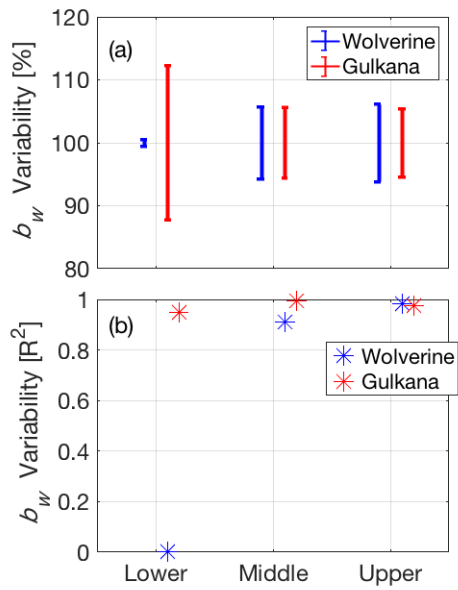
1252
 1253
 1254
 1255
 1256
 1257
 1258
 1259
 1260
 1261
 1262
 1263
 1264
 1265
 1266
 1267

1268 Figure 14. Spatial variability in snow accumulation for individual years (2013-2017) by
 1269 elevation (lower, middle, upper) compared to stake measurements. Box plot of all
 1270 distributed SWE values (from multivariable regression) for each index zone of the glacier
 1271 for Gulkana (a-e) and Wolverine (f-j) for 2013-2017. The filled circles are the respective
 1272 stake observation for that index zone. SWE is expressed as a percentage of the glacier-
 1273 wide average, B_w , for that year and glacier.



1274
 1275
 1276
 1277
 1278
 1279
 1280
 1281
 1282
 1283
 1284
 1285
 1286
 1287
 1288
 1289
 1290
 1291
 1292
 1293

1294 Figure 15. Interannual variability in the spatial pattern of snow accumulation at long-term
 1295 mass balance stake locations for Wolverine and Gulkana glaciers using a) normalized b_w
 1296 range and b) coefficient of determination (from Figure 11; MVR model).
 1297



1298
 1299
 1300
 1301
 1302
 1303
 1304
 1305
 1306
 1307
 1308
 1309